


Detectability of primordial black hole binaries at high redshift

Qianhang Ding^{*}

*Department of Physics, The Hong Kong University of Science and Technology,
Hong Kong, People's Republic of China
and Jockey Club Institute for Advanced Study, The Hong Kong University of Science and Technology,
Hong Kong, People's Republic of China*

 (Received 8 December 2020; revised 27 July 2021; accepted 3 August 2021; published 20 August 2021)

We show that the gravitational wave signals from primordial black hole (PBH) binaries at high redshift can be detected. The detectability of PBH binaries is enhanced by redshift bias and more PBH binaries at high redshift. The initial clustering of PBHs is also included and enhances the effectively detectable mass ranges of PBHs at high redshift. Future observations on the gravitational wave at high redshift by space-based detectors such as the Laser Interferometer Space Antenna (LISA) and Square Kilometre Array (SKA) can constrain the fraction of PBHs in dark matter and PBHs initial distribution.

DOI: [10.1103/PhysRevD.104.043527](https://doi.org/10.1103/PhysRevD.104.043527)

I. INTRODUCTION

Primordial black holes (PBHs) were born from primordial perturbations in highly overdense regions by gravitational collapse [1–3]. Among modern mechanisms of PBHs formation, the inflationary origin [4–8] tightly connects the PBHs properties such as mass distribution [9], abundance distribution [10–13], and the fraction of PBHs in dark matter [14] with the early Universe evolution. Thus, the observational constraint on PBHs provides important clues for inflationary model building. PBHs play an important role in understanding the early Universe. Directly observing signals from PBHs is the key step. In order to achieve that, distinguishing the PBHs and astrophysical black holes is essential. The method to distinguish black holes comes from the black holes intrinsic properties including mass, spin, charge, and spacetime properties such as the spatial distribution and redshift.

One way to distinguish black holes comes from the mass of black holes. The mass of astrophysical black holes is heavier than a particular mass (around 3 solar masses [15,16]). Some specific mechanisms can produce around 1 solar mass astrophysical black holes, see [17,18]. However, PBHs have a different mass range. The mass of a PBH can be roughly estimated as follows [14]:

$$M \sim \frac{c^3 t}{G} \sim 5.03 \times 10^4 \left(\frac{t}{1 \text{ s}} \right) M_{\odot}, \quad (1)$$

where t denotes the time when the corresponding perturbation returns to the horizon. Equation (1) shows that a PBH born before $\mathcal{O}(10^{-4})$ second since the hot big bang

has a mass less than 1 solar mass, which is less than the minimal mass of astrophysical black holes. Considering Hawking radiation [19], PBHs with initial masses of less than 10^{15} g have already evaporated by now; as a result, PBHs with initial masses of more than 10^{15} g and less than 1 solar mass still exist and produce various distinct signals in the present Universe. In detecting sub-solar-mass PBHs, the microlensing effect [20–23], femtolensing effect [24], disruption of white dwarfs [25], disruption of neutron stars [26–28] and so on put constraints on the fraction of sub-solar-mass PBHs in dark matter. Some interactions between black holes and stars can help detect sub-solar-mass PBHs such as superradiance instability around black holes [29,30]. However, these observational effects such as microlensing are extremely weak; only a few events give a weak constraint on the fraction of PBHs in the dark matter.

The other way to distinguish black holes depends on the redshift of signals from black holes. The astrophysical black holes form after the death of Population III stars which are the first generation stars. Their observational signals exist at $z < 20$ [31]. In contrast, the redshift of PBHs goes through the whole history of the Universe after the big bang. From this point, the signals from black holes with $z > 20$ should come from the PBHs. In detecting high redshift signals, the gravitational wave is a powerful detection channel which carries information to travel through cosmological distances due to a weak interaction between gravity and matter. Since the first gravitational wave event from the merger of binary black holes [32], the binary black holes system is the important gravitational wave source, so the detection of gravitational waves from PBH binaries is significant, which can bring us high redshift signals.

Recently, stellar mass PBHs have received renewed interest [33–35] since the gravitational wave events were

^{*}qdingab@connect.ust.hk

detected by the Laser Interferometer Gravitational Wave Observatory (LIGO) [36] and Virgo [37]. Intermediate-mass black holes show clues in LIGO and Virgo detection [38]. A supermassive black hole detection is being discussed [39]. We propose to search for high redshift gravitational wave signals from PBH binaries, which cover a large mass range of PBHs at high redshift. Because the frequency of a gravitational wave from a high redshift source is highly redshifted, the usage of a high frequency ground-based gravitational wave detector is limited. Targeting high redshift signals needs a low frequency space-based gravitational wave detector such as the Laser Interferometer Space Antenna (LISA) [40], DECihertz Interferometer Gravitational Wave Observatory (DECIGO) [41], or Square Kilometre Array (SKA) [42]. The detectability of PBHs shows the possibility in gravitational wave astronomy. There are some existing studies [43,44] about gravitational waves from high redshift PBH binaries. In addition to their studies, we present the potential detectable mass range of PBH binaries at high redshift and include the effect of the initial abundance distribution of PBHs on the detectable mass range.

This paper is organized as follows. In Sec. II, we show that sensitivity of gravitational wave detectors can detect high redshift gravitational waves from binary black holes. In Sec. III, we estimate the event rate of detectable signals from PBH binaries at high redshift. In Sec. IV, we combine the gravitational wave detector sensitivity and PBH binaries event rate to obtain the effectively detectable mass range for PBH binaries at high redshift. We also discuss potential improvements in detectability by the initial clustering of PBHs.

II. GW SENSITIVITY AT HIGH REDSHIFT

The sensitivity of gravitational wave detectors is determined by the amplitude of the gravitational wave and noise strain of the detector. The amplitude of the gravitational wave from the binary system can be expressed as

$$h = \frac{4}{d_L(z)} \left(\frac{GM_c(1+z)}{c^2} \right)^{5/3} \left(\frac{\pi f}{c} \right)^{2/3}. \quad (2)$$

Here, $d_L(z)$ is the luminosity distance of the gravitational wave source in a flat Friedmann-Robertson-Walker (FRW) universe, which can be calculated from $d_L(z) = (1+z) \int_0^z c/H(z') dz'$, G is Newton's constant, c is the speed of light, \mathcal{M}_c is the chirp mass of the binary system, which is defined as $\mathcal{M}_c \equiv (m_1 m_2)^{3/5} / (m_1 + m_2)^{1/5}$, and f is the frequency of the gravitational wave.

The amplitude of the gravitational wave can be boosted by a redshifted chirp mass $(1+z)\mathcal{M}_c$, which introduces an effect called redshift bias [45]. Redshift bias of a rest frame chirp mass can improve the detectability of a binary system at high redshift. It works as follows. The amplitude and frequency of gravitational waves increase with time.

The gravitational wave with higher frequency stays at a later stage in the inspiral phase, which has a larger amplitude than those with low frequency. Then, the frequency of a high redshift gravitational wave is redshifted to the observable frequency at present which follows $f_{\text{rest}} = (1+z)f_{\text{obs}}$. The amplitude of a high redshift gravitational wave also decreases because of the large luminosity distance $d_L(z)$. Consequently, at an observable frequency band, the amplitude of a high redshift gravitational wave depends on two factors: later stage in the inspiral phase and $d_L(z)$, where amplitude first increases and then decreases, which implies that the amplitude of a gravitational wave does not always decrease monotonically with a redshift; it has a minimum value at z_{min} . In the Lambda cold dark matter (Λ CDM) model, $z_{\text{min}} = 2.63$ [45]. Redshift bias can effectively improve the detectability of a gravitational wave at high redshift. This effect is shown in Fig. 1.

In order to detect a gravitational wave event with a high confidence level, the signal-to-noise ratio (SNR) should exceed a threshold during observation. We follow [45], where the optimal SNR is defined as

$$S/N = \sqrt{4 \int_{f_{\text{min}}}^{f_{\text{max}}} \frac{|\tilde{h}(f)|^2}{S_n(f)} df}. \quad (3)$$

Here, $\tilde{h}(f)$ is the Fourier transform of $h(t)$ based on the stationary phase approximation [46], which is

$$\tilde{h}(f) = \sqrt{\frac{5}{24}} \frac{(GM_c(1+z))^{5/6}}{\pi^{2/3} c^{3/2} d_L(z)} f^{-7/6}. \quad (4)$$

The $S_n(f)$ is the noise strain of the detector. The f_{min} is the initial observed frequency, and f_{max} is the final frequency

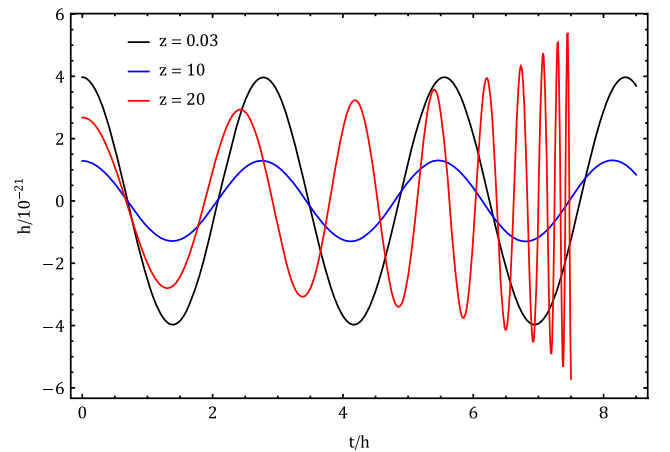


FIG. 1. Gravitational waves with observed frequency 10^{-4} Hz at redshift $z = 0.03, 10, 20$, also see in [45]. The signals at high redshift stay later stage in binary evolution whose frequency is $f_{\text{rest}} = (1+z)f_{\text{obs}}$, which increases the amplitude for observation.

during the observation time, which can be calculated from the evolution of the observed gravitational wave frequency,

$$\frac{df}{dt} = \frac{96\pi^{8/3}(GM_c(1+z))^{5/3}}{5c^5} f(t)^{11/3}. \quad (5)$$

The optimal signal-to-noise ratio should exceed a conservative threshold of 8, which makes sure the detection probability is $> 95\%$ and a false alarm probability of $< 0.1\%$.

Due to the redshift bias effect, S/N doesn't always decrease monotonically with redshift. It also has a minimal value at z_{\min} . When $z < z_{\min}$, optimal SNR decreases with z . Otherwise, optimal SNR increases with z for the case $z > z_{\min}$. In order to obtain z_{\min} , we need to calculate $\partial(S/N)^2/\partial z = 0$, which can be expressed as the following:

$$\frac{\partial S/N^2}{\partial z} = 4 \int_{t_{\min}}^{t_{\max}} \frac{1}{S_n(f)} \frac{\partial}{\partial z} \left(|\tilde{h}(f)|^2 \frac{df}{dt} \right) dt = 0. \quad (6)$$

Applying Eqs. (4) and (5) into Eq. (6), we can get the equation for z_{\min} ,

$$(1 + z_{\min}) \left. \frac{\partial \ln d_L(z)}{\partial z} \right|_{z_{\min}} = \frac{5}{3}. \quad (7)$$

In the Λ CDM model with $\Omega_m = 0.315$ and $\Omega_\Lambda = 0.685$ [47], $z_{\min} = 2.63$. Figure 2 of [45] shows the same result.

Combining Eqs. (3), (4), and (5) with the condition $S/N > 8$, we can get the detectable mass ranges at different redshifts in Fig. 2. In order to observe the mass range as large as possible, the frequency range in Eq. (3)

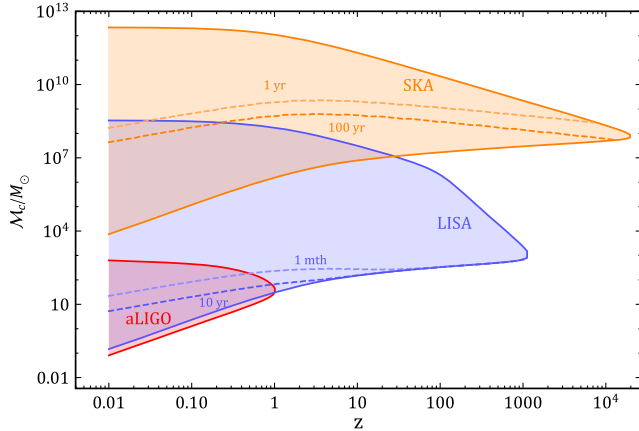


FIG. 2. The detectable mass range at different redshifts for gravitational wave detectors aLIGO, LISA, and SKA. The SNR of each binary (M_c, z) is larger than the threshold of 8. The typical observation times of 1 month and 10 years for LISA and 1 year and 100 years for SKA are shown as dashed lines, where $S/N = 8$. The shadow regions above the dashed lines show the detectable mass ranges within different observation times.

between f_{\min} and f_{\max} should be large so that $S/N > 8$. We set the f_{\min} as the minimal detectable frequency of the detector. The f_{\max} is set to the minimal quantity between the maximal detectable frequency of the detector and the maximal redshifted inspiral phase frequency $f_{\text{insp}}^{\max}/(1+z)$ Hz. Here, the maximal inspiral phase frequency in the rest frame can be estimated as $f_{\text{insp}}^{\max} = (a\eta^2 + b\eta + c)/\pi GM$ [48–50]. The symmetric mass ratio η is defined as $\eta \equiv m_1 m_2 / M^2$ and $M \equiv m_1 + m_2$, and the coefficients are $a = 0.29740$, $b = 0.04481$, and $c = 0.09556$ (see Table 1 of [51]). The $S_n(f)$ for each detector can be obtained from Fig. A2 in [52].

In Fig. 2, there is a redshift range corresponding with a PBH mass. For low mass PBH binaries, the amplitude of the gravitational wave is small, which needs a higher f_{\max} to increase SNR; then, the maximal detectable redshift should be small so that f_{\max} is not compressed by $f_{\text{insp}}^{\max}/(1+z)$ Hz. The boundary of the shadow region corresponds with $S/N = 8$. The PBH binary at higher redshift cannot be detected due to the condition $f_{\min} \geq f_{\max}$ in Eq. (3), which results from the maximal inspiral frequency of a binary system being redshifted that is less than the minimal frequency of the detector. For a practical observation, the observation time T_{obs} is limited, so we choose different observation times to determine the frequency range as follows:

$$f_{\max} - f_{\min} = \int_{t_{\min}}^{t_{\min} + T_{\text{obs}}} \frac{df}{dt} dt. \quad (8)$$

The f_{\min} is chosen from the frequency band of the detector; then, f_{\max} can be obtained from Eq. (8). The typical observation time is shown as a dashed line in Fig. 2. The shadow regions above the dashed lines show detectable mass ranges of detectors within the observation time. We find that the dashed lines are not monotonic, which is caused by the redshift bias effect. According to Eqs. (6) and (7), the optimal SNR function is monotonically decreasing for $z < 2.63$ and increasing for $z > 2.63$ in our Λ CDM universe [47]; for detecting the signal with $S/N = 8$, the chirp mass of the PBH binary needs increased for $z < 2.63$ and decreased for $z > 2.63$.

III. EVENT RATE OF PBH BINARIES

In order to observe the PBHs at high redshift, not only should gravitational wave sensitivity be high but also the event rate of the PBH binaries system should be large enough. The estimation of a PBH binaries event rate follows [35], and the condition for decoupling of the PBH binaries from the FRW background at matter-radiation equality $z = z_{\text{eq}}$ is

$$x < f_{\text{PBH}}^{1/3} \bar{x}. \quad (9)$$

Here, x is the physical distance between two nearby black holes, and f_{PBH} is the fraction of PBHs in the dark matter. \bar{x} is the mean separation of PBHs at matter-radiation equality, which is determined by PBH mass M_{BH} and energy density $\rho_{\text{BH}}(z_{\text{eq}})$ as $\bar{x} = (M_{\text{BH}}/\rho_{\text{BH}}(z_{\text{eq}}))^{1/3}$. After interacting with the third black hole, the probability distribution function of a binary system with respect to the major axes a and eccentricity e [35] is

$$P(a, e) = \frac{3 f_{\text{PBH}}^{3/2} a^{1/2}}{4 \bar{x}^{3/2}} \frac{e}{(1 - e^2)^{3/2}}. \quad (10)$$

After long time evolution, the major axes shrinks to a suitable quantity that the frequency of the gravitational wave lies in the frequency the band of detector. Following [53,54], we assume that e keeps the constant during the inspiral phase, and the later major axes can be expressed as

$$a^4 = a_{\text{ini}}^4 - \frac{256}{5} \frac{G^3 \mu M^2}{c^5 (1 - e^2)^{7/2}} t, \quad (11)$$

where a_{ini} is the initial major axes of PBH binary, t is the evolution time, $M \equiv m_1 + m_2$, and $\mu \equiv m_1 m_2 / M$. Applying Kepler's third law with Eq. (11), Eq. (10) can be written as

$$P(t, e) = \frac{48 f_{\text{PBH}}^{3/2} G^3 \mu M^2}{5 c^5 \bar{x}^{3/2} T^{5/8}} \frac{e}{(1 - e^2)^5}. \quad (12)$$

Here, T is defined as

$$T \equiv \left(\frac{GM}{\pi^2 f_{\text{GW}}^2} \right)^{4/3} + \frac{256}{5} \frac{G^3 \mu M^2}{c^5 (1 - e^2)^{7/2}} t. \quad (13)$$

where f_{GW} is the frequency of gravitational waves. Then, integrate the e from 0 to the maximum eccentricity to get a probability distribution function of time $P(t)$; the maximum eccentricity is determined by binary formation conditions in [35].

The event rate of gravitational wave signals from PBH binaries can be calculated from $P(t)$ and the average number density of PBHs in a comoving volume n_{BH} ,

$$\text{event rate} = n_{\text{BH}} P(t) = \frac{3H_0^2 \Omega_{\text{BH}}}{8\pi G M_{\text{BH}}} P(t). \quad (14)$$

In order to obtain the event rate at different redshifts, the time-redshift relation along the line of sight is required, which can be calculated from

$$t(z) = \int_z^\infty \frac{dz'}{H(z')(1+z')}. \quad (15)$$

Applying Eq. (15) into $P(t)$, we can get the event rate of PBH binary at different redshifts in Fig. 3. It shows the increasing event rate of PBH binaries at higher redshift.

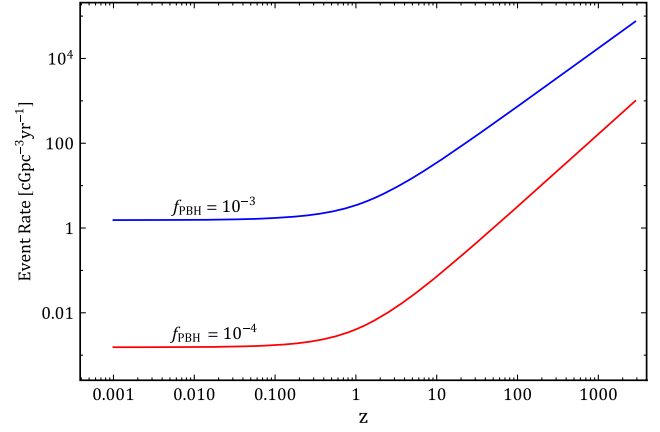


FIG. 3. The event rate for PBH binaries with 100 solar masses and the observed frequency is 10^{-4} Hz at different redshifts. The event rate is measured in a comoving volume with the unit of $\text{cGpc}^{-3} \text{yr}^{-1}$.

This is caused by $P(a) \propto a^{-1/4}$ [35]; there are more PBH binaries having small major axes, when binaries form, which emit high frequency gravitational waves and merge at high redshifts. So more high frequency gravitational wave events propagate from high redshifts to the present that are redshifted and lie in the frequency band of detectors (also see in [55,56]).

More event rates of PBH binaries at high redshift in Fig. 3 show that it is possible to detect the signal from PBH binaries at high redshift, even though the fraction of PBHs in dark matter f_{PBH} is strongly constrained by astronomy observation. Then, we can compare the high redshift $f_{\text{PBH}} - M_{\text{BH}}$ relation with the astronomy observation. Here, we consider the monochromatic PBH mass function in Eq. (14). Considering that the detectable merger rate of binary black holes is $2 - 53 \text{cGpc}^{-3} \text{yr}^{-1}$ for aLIGO [57], a reasonable and detectable event rate is set to $1 \text{cGpc}^{-3} \text{yr}^{-1}$. Then we can get the relation among the fraction of PBHs in dark matter f_{PBH} , PBH mass M_{BH} , and redshift z from Eq. (14), which is shown in Fig. 4. Three typical redshift curves $z = 0, 20, 2000$ are shown, which correspond with a fixed event rate $1 \text{cGpc}^{-3} \text{yr}^{-1}$. We can find that at the same M_{BH} and a higher redshift, the lower f_{PBH} we need to reach an detectable event rate of $1 \text{cGpc}^{-3} \text{yr}^{-1}$, which means high redshift PBH binaries can be detected without ruling out astronomy constraints. It results because there are more event rates at high redshift when we fix f_{PBH} as shown in Fig. 3. Then, we do not need a large f_{PBH} to produce an detectable event rate of $1 \text{cGpc}^{-3} \text{yr}^{-1}$ at high redshift.

IV. DETECTABLE MASS RANGE AT HIGH REDSHIFT

Above all, we have discussed the detectable mass ranges of detectors aLIGO, LISA, SKA, and the event rate of PBH binaries at different redshifts. Now, we can combine the

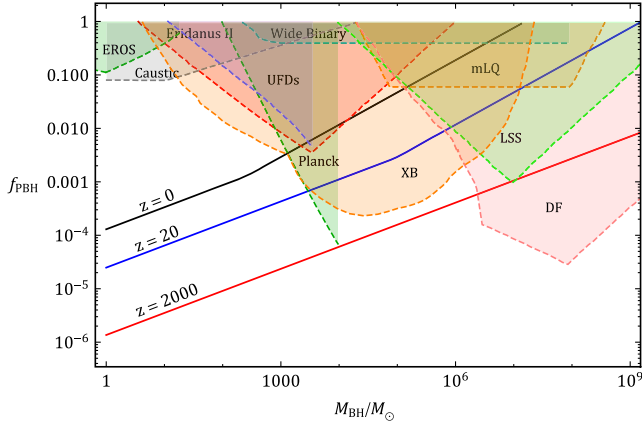


FIG. 4. The fraction of PBHs in dark matter with respect to PBH mass M_{BH} at different redshifts to reach an event rate of $1\text{Gpc}^{-3}\text{yr}^{-1}$. Limits from Experience pour la Recherche d’Objets Sombres (EROS) [58], Caustic [59], ultra-faint dwarfs (UFDs) [60], Eridanus II [60], Planck [61], wide-binary disruption [62], and accretion limits come from X-ray binaries [63], millilensing of quasars [64], generation of large-scale structures through Poisson fluctuations [65], and dynamical friction on halo objects [66] are also plotted.

two results to obtain the effectively detectable region for PBHs at different redshifts as shown in Fig. 5.

In drawing the effective regions, we assume the effectively detectable range follows the conditions,

$$\text{event rate} > 1\text{Gpc}^{-3}\text{yr}^{-1}, \quad f_{\text{PBH}} < f_{\text{unc}}. \quad (16)$$

Here, we follow [13,57], the minimal detectable event rate is set to $1\text{Gpc}^{-3}\text{yr}^{-1}$. f_{unc} is the unconstrained fraction of PBHs in the dark matter where we take 10^{-3} , 10^{-4} , and

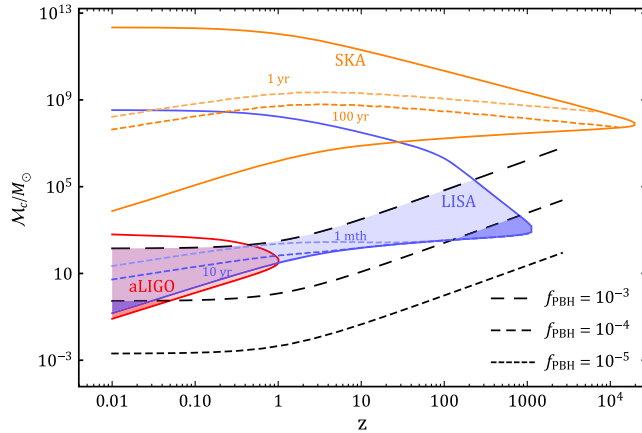


FIG. 5. The effectively detectable regions for PBH binaries at different redshifts. The solid lines give the boundaries of parameter regions that detectors can observe. The black dashed lines give the critical mass with an event rate of $1\text{Gpc}^{-3}\text{yr}^{-1}$ that we can observe for different f_{PBH} . The shadow regions below the black dashed lines and above the solid lines are the effectively detectable regions for PBH binaries.

10^{-5} for illustration. The black dashed lines correspond with an event rate of $1\text{Gpc}^{-3}\text{yr}^{-1}$. The shadow regions show the effectively detectable mass ranges at high redshift. One thing we need to pay attention to is that the maximum detectable redshift is $z = 3000$, which comes from the PBH binary model [35]; the PBH binaries formed at matter-radiation equality $z_{\text{eq}} = 3000$. This mechanism can hardly produce PBHs in a radiation-domination epoch at $z > z_{\text{eq}}$, which makes it difficult to observe a larger mass range and detecting PBH binaries on SKA.

The inclusion of initial spatial clustering of PBHs changes the story. The initial clustering of PBHs forms high density PBHs regions in a radiation-domination epoch. As we have shown in [13], the initial clustering of PBHs can be constructed in multi-stream inflation [67–70]. During multi-stream inflation, inflaton travels along two inflation trajectories. Inflation potential on one trajectory can produce PBHs; the others cannot produce PBHs. In the PBHs clustering model [13], the PBHs clustering regions are denoted by β , which is the volume fraction of PBHs regions in the observed Universe. The redshift of matter-radiation equality in PBHs-rich regions can be calculated by increasing the PBHs fraction in dark matter in PBHs-rich regions $f_{\text{PBH}} \rightarrow f_{\text{PBH}}/\beta$ as follows:

$$1 + z_{\text{PBH,eq}} = \left(1 - f_{\text{PBH}} + \frac{f_{\text{PBH}}}{\beta}\right)(1 + z_{\text{eq}}). \quad (17)$$

The high density PBHs region improves the probability of PBH binaries formation by increasing the PBHs density. Then, event rate of PBH binaries can be enhanced due to a

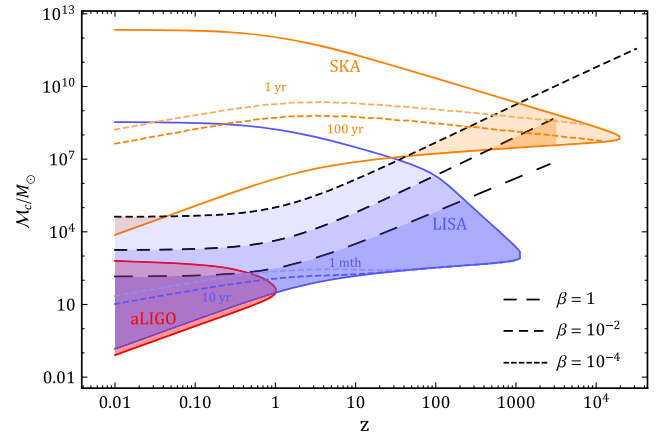


FIG. 6. The effectively detectable regions for PBH binaries at different redshifts with initial clustering. The solid lines give the boundaries of parameter regions that detectors can observe. The black dashed lines give the critical mass with an event rate of $1\text{Gpc}^{-3}\text{yr}^{-1}$ and $f_{\text{PBH}} = 10^{-3}$ that we can observe for different β . The shadow regions below the black dashed lines and above the solid lines are the effectively detectable regions for PBH binaries.

larger PBH binaries density, which results in massive PBH binaries meeting Eq. (16), and the result is shown in Fig. 6. The initial clustering of PBHs expands the detectable mass range for PBH binaries and improves the detectability of PBH binaries in SKA. However, the clustering volume fraction β cannot be infinitesimal, this could result in few PBHs surviving at present, and most of them merged at very high redshift, which leaves weak signals to detectors.

V. CONCLUSION

In this paper, we show that the PBH binaries can be detected by high redshift $z > 20$ gravitational wave signals. During the propagation of gravitational waves from high redshift to the present, the frequency of a gravitational wave is decreasing so that it lies in the frequency band of gravitational wave detectors. Then, the amplitude of redshifted high frequency gravitational waves can significantly enhance the S/N at $z > z_{\min}$, where $z_{\min} = 2.63$ in the Λ CDM model. This phenomena are studied in detail in [45]. In order to detect gravitational wave signals from PBH binaries within practical observation time, the event rate of a gravitational wave from PBH binaries is estimated. We consider the model in [35], and the PBH binaries events are enhanced at high redshift which can achieve $90\text{cGpc}^{-3}\text{yr}^{-1}$ at $z = 20$ for PBHs masses of 100 solar masses with $f_{\text{PBH}} = 10^{-3}$ in Fig. 3. The enhancement of gravitational wave signals and the event rate from PBH binaries at high redshift improve the detectability of PBH binaries. Then, we study the effect of initial clustering of PBHs on its detectability as we have studied in [13]. An enhancement in effectively detectable mass ranges appears by the initial clustering of PBHs. The effectively observable mass range covers $20 - 10^3$ solar masses at $z = 20$ within 10 years observation time on LISA. This mass range can be enhanced to $20 - 10^6$ solar masses with initial clustering of

$\beta = 10^{-4}$. The wide mass range shows that it is possible to detect the PBH binaries on LISA and SKA at high redshift.

Based on the possibility of PBH binaries detection at high redshift, we can directly observe the signals from the PBHs. This can help us build an early Universe model. The mass function of PBHs can be obtained from the chirp mass of gravitational wave in the rest frame and gives clues to the inflation potential [9]. The abundance distribution of PBHs can be obtained from the position distribution of gravitational wave events, which gives a hint of the inflation model with position properties, such as the initial clustering of PBHs from multi-stream inflation [13]. The fraction of PBHs in the dark matter can be constrained by the high redshift gravitational wave event rate, which can tell us the potential dark matter candidates.

In this work, we only consider the monochromatic PBH mass function. The extended mass function of PBHs can form extreme mass ratio inspirals, which can produce different signals. In detecting more PBHs events at high redshift, the stochastic gravitational wave background from PBHs formation needs to be deducted [71–73]. Due to the high redshift of the gravitational wave, no electromagnetic counterpart can be observed along with the gravitational wave signal. We cannot directly observe the luminosity distance of gravitational waves. However, the interaction between Population III stars with PBHs could be a potential source for electromagnetic signals at $z < 20$, which helps us understand PBHs evolution at high redshift.

ACKNOWLEDGMENTS

The author thanks Yi Wang for detailed suggestions and Lingfeng Li and Xi Tong for useful comments. The author also thanks Xingwei Tang for her kind encouragement and suggestions.

-
- [1] S. Hawking, Gravitationally collapsed objects of very low mass, *Mon. Not. R. Astron. Soc.* **152**, 75 (1971).
 - [2] Y. B. Zel'dovich and I. D. Novikov, The hypothesis of cores retarded during expansion and the hot cosmological model, *Astron. Zh.* **43**, 758 (1966); *Sov. Astron.* **10**, 602 (1967).
 - [3] B. J. Carr and S. W. Hawking, Black holes in the early Universe, *Mon. Not. R. Astron. Soc.* **168**, 399 (1974).
 - [4] J. Yokoyama, Formation of MACHO primordial black holes in inflationary cosmology, *Astron. Astrophys.* **318**, 673 (1997).
 - [5] J. Yokoyama, Chaotic new inflation and formation of primordial black holes, *Phys. Rev. D* **58**, 083510 (1998).
 - [6] M. Kawasaki, A. Kusenko, Y. Tada, and T. T. Yanagida, Primordial black holes as dark matter in supergravity inflation models, *Phys. Rev. D* **94**, 083523 (2016).
 - [7] K. Inomata, M. Kawasaki, K. Mukaida, Y. Tada, and T. T. Yanagida, Inflationary primordial black holes for the LIGO gravitational wave events and pulsar timing array experiments, *Phys. Rev. D* **95**, 123510 (2017).
 - [8] Y. F. Cai, X. Tong, D. G. Wang, and S. F. Yan, Primordial Black Holes from Sound Speed Resonance During Inflation, *Phys. Rev. Lett.* **121**, 081306 (2018).
 - [9] S. Young, C. T. Byrnes, and M. Sasaki, Calculating the mass fraction of primordial black holes, *J. Cosmol. Astropart. Phys.* **07** (2014) 045.
 - [10] K. M. Belotsky, A. D. Dmitriev, E. A. Esipova, V. A. Gani, A. V. Grobov, M. Y. Khlopov, A. A. Kirillov, S. G. Rubin, and I. V. Svadkovsky, Signatures of primordial black hole dark matter, *Mod. Phys. Lett. A* **29**, 1440005 (2014).

- [11] K. M. Belotsky, V. I. Dokuchaev, Y. N. Eroshenko, E. A. Esipova, M. Y. Khlopov, L. A. Khromykh, A. A. Kirillov, V. V. Nikulin, S. G. Rubin, and I. V. Svadkovsky, Clusters of primordial black holes, *Eur. Phys. J. C* **79**, 246 (2019).
- [12] T. Bringmann, P. F. Depta, V. Domcke, and K. Schmidt-Hoberg, Towards closing the window of primordial black holes as dark matter: The case of large clustering, *Phys. Rev. D* **99**, 063532 (2019).
- [13] Q. Ding, T. Nakama, J. Silk, and Y. Wang, Detectability of gravitational waves from the coalescence of massive primordial black holes with initial clustering, *Phys. Rev. D* **100**, 103003 (2019).
- [14] B. Carr, F. Kuhnel, and M. Sandstad, Primordial black holes as dark matter, *Phys. Rev. D* **94**, 083504 (2016).
- [15] C. E. Rhoades, Jr. and R. Ruffini, Maximum Mass of a Neutron Star, *Phys. Rev. Lett.* **32**, 324 (1974).
- [16] V. Kalogera and G. Baym, The maximum mass of a neutron star, *Astrophys. J. Lett.* **470**, L61 (1996).
- [17] C. Kouvaris, P. Tinyakov, and M. H. G. Tytgat, Non-Primordial Solar Mass Black Holes, *Phys. Rev. Lett.* **121**, 221102 (2018).
- [18] B. Dasgupta, R. Laha, and A. Ray, Low Mass Black Holes from Dark Core Collapse, *Phys. Rev. Lett.* **126**, 141105 (2021).
- [19] S. W. Hawking, Black hole explosions, *Nature (London)* **248**, 30 (1974).
- [20] B. Paczynski, Gravitational microlensing by the galactic halo, *Astrophys. J.* **304**, 1 (1986).
- [21] C. Alcock *et al.* (Supernova Cosmology Project Collaboration), Possible gravitational microlensing of a star in the large magellanic cloud, *Nature (London)* **365**, 621 (1993).
- [22] E. Aubourg, P. Bareyre, S. Brehin, M. Gros, M. Lachieze-Rey, B. Laurent, E. Lesquoy, C. Magneville, A. Milsztain, L. Moscoso *et al.*, Evidence for gravitational microlensing by dark objects in the galactic halo, *Nature (London)* **365**, 623 (1993).
- [23] C. Alcock *et al.* (MACHO Collaboration), The MACHO project: Microlensing results from 5.7 years of LMC observations, *Astrophys. J.* **542**, 281 (2000).
- [24] A. Barnacka, J. F. Glicenstein, and R. Moderski, New constraints on primordial black holes abundance from femtolensing of gamma-ray bursts, *Phys. Rev. D* **86**, 043001 (2012).
- [25] P. W. Graham, S. Rajendran, and J. Varela, Dark matter triggers of supernovae, *Phys. Rev. D* **92**, 063007 (2015).
- [26] F. Capela, M. Pshirkov, and P. Tinyakov, Constraints on primordial black holes as dark matter candidates from capture by neutron stars, *Phys. Rev. D* **87**, 123524 (2013).
- [27] C. Kouvaris and P. Tinyakov, Growth of black holes in the interior of rotating neutron stars, *Phys. Rev. D* **90**, 043512 (2014).
- [28] P. Pani and A. Loeb, Tidal capture of a primordial black hole by a neutron star: Implications for constraints on dark matter, *J. Cosmol. Astropart. Phys.* **06** (2014) 026.
- [29] D. Baumann, H. S. Chia, R. A. Porto, and J. Stout, Gravitational collider physics, *Phys. Rev. D* **101**, 083019 (2020).
- [30] Q. Ding, X. Tong, and Y. Wang, Gravitational collider physics via pulsar-black hole binaries, *Astrophys. J.* **908**, 78 (2021).
- [31] N. Yoshida, V. Bromm, and L. Hernquist, The era of massive population III stars: Cosmological implications and self-termination, *Astrophys. J.* **605**, 579 (2004).
- [32] B. P. Abbott *et al.* (LIGO Scientific and Virgo Collaborations), Observation of Gravitational Waves from a Binary Black Hole Merger, *Phys. Rev. Lett.* **116**, 061102 (2016).
- [33] S. Bird, I. Cholis, J. B. Muñoz, Y. Ali-Haïmoud, M. Kamionkowski, E. D. Kovetz, A. Raccanelli, and A. G. Riess, Did LIGO Detect Dark Matter? *Phys. Rev. Lett.* **116**, 201301 (2016).
- [34] S. Clesse and J. García-Bellido, The clustering of massive primordial black holes as dark matter: Measuring their mass distribution with Advanced LIGO, *Phys. Dark Universe* **15**, 142 (2017).
- [35] M. Sasaki, T. Suyama, T. Tanaka, and S. Yokoyama, Primordial Black Hole Scenario for the Gravitational-Wave Event GW150914, *Phys. Rev. Lett.* **117**, 061101 (2016); Erratum, *Phys. Rev. Lett.* **121**, 059901 (2018).
- [36] B. P. Abbott *et al.* (LIGO Scientific Collaboration), LIGO: The laser interferometer gravitational-wave observatory, *Rep. Prog. Phys.* **72**, 076901 (2009).
- [37] F. Acernese *et al.* (VIRGO Collaboration), Advanced Virgo: A second-generation interferometric gravitational wave detector, *Classical Quantum Gravity* **32**, 024001 (2015).
- [38] R. Abbott *et al.* (LIGO Scientific and Virgo Collaborations), GW190521: A Binary Black Hole Merger with a Total Mass of $150 M_{\odot}$, *Phys. Rev. Lett.* **125**, 101102 (2020).
- [39] Z. Arzoumanian *et al.* (NANOGrav Collaboration), The NANOGrav 12.5-year data set: Search for an isotropic stochastic gravitational-wave background, *Astrophys. J. Lett.* **905**, L34 (2020).
- [40] P. L. Bender *et al.*, LISA Pre-Phase A Report; Second Edition, MPQ 233 (1998).
- [41] S. Kawamura, T. Nakamura, M. Ando, N. Seto, K. Tsubono, K. Numata, R. Takahashi, S. Nagano, T. Ishikawa, M. Musha *et al.*, The Japanese space gravitational wave antenna DECIGO, *Classical Quantum Gravity* **23**, S125 (2006).
- [42] P. E. Dewdney, P. J. Hall, R. T. Schilizzi, and T. J. L. Lazio, The square kilometre array, *Proce. IEEE* **97**, 1482 (2009).
- [43] T. Nakamura, M. Ando, T. Kinugawa, H. Nakano, K. Eda, S. Sato, M. Musha, T. Akutsu, T. Tanaka, N. Seto *et al.*, Pre-DECIGO can get the smoking gun to decide the astrophysical or cosmological origin of GW150914-like binary black holes, *Prog. Theor. Exp. Phys.* (2016), 093E01.
- [44] V. Mandic, S. Bird, and I. Cholis, Stochastic Gravitational-Wave Background Due to Primordial Binary Black Hole Mergers, *Phys. Rev. Lett.* **117**, 201102 (2016).
- [45] P. A. Rosado, P. D. Lasky, E. Thrane, X. Zhu, I. Mandel, and A. Sesana, Detectability of Gravitational Waves from High-Redshift Binaries, *Phys. Rev. Lett.* **116**, 101102 (2016).
- [46] S. Droz, D. J. Knapp, E. Poisson, and B. J. Owen, Gravitational waves from inspiraling compact binaries: Validity of the stationary phase approximation to the Fourier transform, *Phys. Rev. D* **59**, 124016 (1999).
- [47] N. Aghanim *et al.* (Planck Collaboration), Planck 2018 results. VI. Cosmological parameters, *Astron. Astrophys.* **641**, A6 (2020).
- [48] D. F. Chernoff and L. S. Finn, Gravitational radiation, inspiraling binaries, and cosmology, *Astrophys. J. Lett.* **411**, L5 (1993).

- [49] P. Ajith, M. Hannam, S. Husa, Y. Chen, B. Bruegmann, N. Dorband, D. Muller, F. Ohme, D. Pollney, C. Reisswig *et al.*, Inspiral-Merger-Ringdown Waveforms for Black-Hole Binaries with Non-Precessing Spins, *Phys. Rev. Lett.* **106**, 241101 (2011).
- [50] X. J. Zhu, E. Howell, T. Regimbau, D. Blair, and Z. H. Zhu, Stochastic gravitational wave background from coalescing binary black holes, *Astrophys. J.* **739**, 86 (2011).
- [51] P. Ajith, S. Babak, Y. Chen, M. Hewitson, B. Krishnan, A. M. Sintes, J. T. Whelan, B. Bruegmann, P. Diener, N. Dorband *et al.*, A template bank for gravitational waveforms from coalescing binary black holes. I. Non-spinning binaries, *Phys. Rev. D* **77**, 104017 (2008); Erratum, *Phys. Rev. D* **79**, 129901 (2009).
- [52] C. J. Moore, R. H. Cole, and C. P. L. Berry, Gravitational-wave sensitivity curves, *Classical Quantum Gravity* **32**, 015014 (2015).
- [53] P. C. Peters and J. Mathews, Gravitational radiation from point masses in a Keplerian orbit, *Phys. Rev.* **131**, 435 (1963).
- [54] P. C. Peters, Gravitational radiation and the motion of two point masses, *Phys. Rev.* **136**, B1224 (1964).
- [55] Y. Ali-Haïmoud, E. D. Kovetz, and M. Kamionkowski, Merger rate of primordial black-hole binaries, *Phys. Rev. D* **96**, 123523 (2017).
- [56] B. J. Kavanagh, D. Gaggero, and G. Bertone, Merger rate of a subdominant population of primordial black holes, *Phys. Rev. D* **98**, 023536 (2018).
- [57] B. P. Abbott *et al.* (LIGO Scientific and Virgo Collaborations), The rate of binary black hole mergers inferred from advanced LIGO observations surrounding GW150914, *Astrophys. J. Lett.* **833**, L1 (2016).
- [58] P. Tisserand *et al.* (EROS-2 Collaboration), Limits on the macho content of the galactic halo from the EROS-2 survey of the magellanic clouds, *Astron. Astrophys.* **469**, 387 (2007).
- [59] M. Oguri, J. M. Diego, N. Kaiser, P. L. Kelly, and T. Broadhurst, Understanding caustic crossings in giant arcs: Characteristic scales, event rates, and constraints on compact dark matter, *Phys. Rev. D* **97**, 023518 (2018).
- [60] T. D. Brandt, Constraints on MACHO dark matter from compact stellar systems in ultra-faint dwarf galaxies, *Astrophys. J. Lett.* **824**, L31 (2016).
- [61] Y. Ali-Haimoud and M. Kamionkowski, Cosmic microwave background limits on accreting primordial black holes, *Phys. Rev. D* **95**, 043534 (2017).
- [62] D. P. Quinn, M. I. Wilkinson, M. J. Irwin, J. Marshall, A. Koch, and V. Belokurov, On the reported death of the MACHO era, *Mon. Not. R. Astron. Soc.* **396**, L11 (2009).
- [63] Y. Inoue and A. Kusenko, New X-ray bound on density of primordial black holes, *J. Cosmol. Astropart. Phys.* **10** (2017) 034.
- [64] P. N. Wilkinson, D. R. Henstock, I. W. A. Browne, A. G. Polatidis, P. Augusto, A. C. S. Readhead, T. J. Pearson, W. Xu, G. B. Taylor, and R. C. Vermeulen, Limits on the Cosmological Abundance of Supermassive Compact Objects from a Search for Multiple Imaging in Compact Radio Sources, *Phys. Rev. Lett.* **86**, 584 (2001).
- [65] N. Afshordi, P. McDonald, and D. N. Spergel, Primordial black holes as dark matter: The power spectrum and evaporation of early structures, *Astrophys. J. Lett.* **594**, L71 (2003).
- [66] B. J. Carr and M. Sakellariadou, Dynamical constraints on dark compact objects, *Astrophys. J.* **516**, 195 (1999).
- [67] M. Li and Y. Wang, Multi-stream inflation, *J. Cosmol. Astropart. Phys.* **07** (2009) 033.
- [68] S. Li, Y. Liu, and Y. S. Piao, Inflation in web, *Phys. Rev. D* **80**, 123535 (2009).
- [69] Y. Wang, Multi-stream inflation: Bifurcations and recombinations in the multiverse, [arXiv:1001.0008](https://arxiv.org/abs/1001.0008).
- [70] N. Afshordi, A. Slosar, and Y. Wang, A theory of a spot, *J. Cosmol. Astropart. Phys.* **01** (2011) 019.
- [71] S. Wang, Y. F. Wang, Q. G. Huang, and T. G. F. Li, Constraints on the Primordial Black Hole Abundance from the First Advanced LIGO Observation Run Using the Stochastic Gravitational-Wave Background, *Phys. Rev. Lett.* **120**, 191102 (2018).
- [72] Y. F. Cai, C. Chen, X. Tong, D. G. Wang, and S. F. Yan, When primordial black holes from sound speed resonance meet a stochastic background of gravitational waves, *Phys. Rev. D* **100**, 043518 (2019).
- [73] T. Nakama, Stochastic gravitational waves associated with primordial black holes formed during an early matter era, *Phys. Rev. D* **101**, 063519 (2020).